Journal of the European Ceramic Society xxx (xxxx) xxx

Contents lists available at ScienceDirect

Journal of the European Ceramic Society

journal homepage: www.elsevier.com/locate/jeurceramsoc

Highly porous Sr-doped TiO_2 ceramics maintain compressive strength after grain boundary corrosion

Anne Klemm, Hanna Tiainen *

Department of Biomaterials, Institute of Clinical Dentistry, University of Oslo, Norway

ARTICLE INFO

Keywords:
Grain boundaries
Titanium dioxide
Bone scaffolds
Porous ceramics
Sintering

ABSTRACT

Maintaining sufficient mechanical support during bone healing is an essential property for ceramic bone scaffolds. However, grain boundary (GB) dissolution may compromise the mechanical strength of polycrystalline ceramics in the physiological environment. Therefore, we investigated the GB formation and its impact on the compressive strength and corrosion behavior in TiO_2 scaffolds doped with calcium and strontium. To alter the GB composition and densification process, sintering conditions were altered. Prolonged sintering times and increased sintering temperature led to improved densification and increased strength in Ca-doped scaffolds. However, dissolution of the resulting amorphous GBs caused a significant loss of compressive strength when exposed to an acidic environment. In contrast, a crystalline $SrTiO_3$ GB phase present in Sr-doped scaffolds, for which increased sintering temperature combined with rapid cooling led to a significantly improved compressive strength. Formation of $SrTiO_3$ crystals in the GBs maintained the strength for over 4 weeks in an acidic environment.

1. Introduction

Ceramic titanium dioxide (TiO_2) foams have excellent characteristics to be used in different applications such as catalysts in air and water purification systems, diesel particulate filters and also as bone graft materials [1–8]. High compressive strength combined with high porosity and interconnected pore space are necessary properties for the foam in all of these different applications. However, the ability to form a hydroxyapatite layer, which enables a direct strong bond to bone, makes TiO_2 highly suitable as a bone graft material [9]. Additionally, the highly interconnected pore structure of TiO_2 foam enables vascularisation and osteogenesis within the entire scaffold volume [6,10]. Despite their high interconnected porosity, TiO_2 foams have compressive strength that is comparable to human trabecular bone, making TiO_2 scaffolds suitable for bone tissue engineering applications [5]. However, exposure to an acidic environment can result in a dramatic loss of compressive strength [11,12]. During the inflammatory phase of the bone remodeling process, macrophages and osteoclasts acidify the microenvironment at the bone defect site [13,14]. This aggressive chemical environment can cause dissolution of poorly crystalline ceramic grain boundaries, and thus, result in a significant loss in compressive strength [11,15,16]. Consequently, other studies have focused on the protection of grain boundaries to prevent corrosion in ceramics [17–20]. Coatings for example provide an easy method to protect grain boundaries. However, considering the complex 3D structure of high porous scaffolds, producing a homogeneous coating is challenging and the risk of inhomogeneity and cracks is high. Thus, other techniques need to be investigated to protect the grain boundaries from the external environment and thus prevent corrosion.

The present study focused on investigating the influence of amorphous and crystalline phases on grain boundary corrosion in highly porous TiO_2 scaffolds doped with calcium and strontium. The formation and morphological structure of the grain boundary phase forming during sintering in these ceramics were assessed following sintering of the ceramic foams under different sintering conditions using electron microscopy. Since the grain boundaries, and particularly, their dissolution in aggressive environments can have a detrimental impact on the mechanical integrity of highly porous scaffolds [11,12], the mechanical properties of the produced scaffolds were tested before and after exposure to 1 mM HCl to assess the influence of altered sintering conditions on the corrosion resistance of the formed grain boundary phase.

* Corresponding author.
E-mail address: hanna.tiainen@odont.uio.no (H. Tiainen).

https://doi.org/10.1016/j.jeurceramsoc.2021.04.059
Received 28 January 2021; Received in revised form 29 April 2021; Accepted 30 April 2021
Available online 4 May 2021

Please cite this article as: Anne Klemm, Hanna Tiainen, *Journal of the European Ceramic Society*, https://doi.org/10.1016/j.jeurceramsoc.2021.04.059

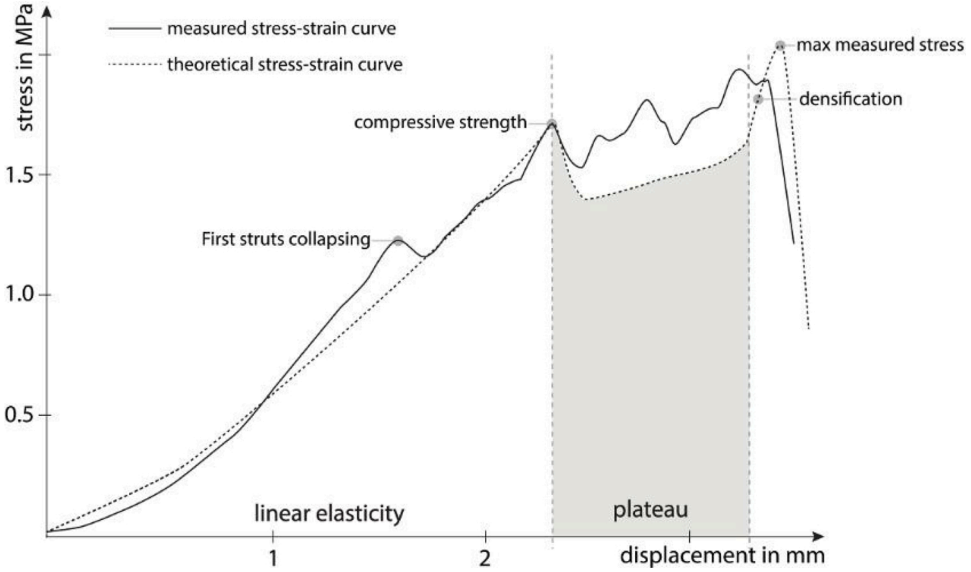

Fig. 1. A representative stress-displacement curve for highly porous TiO_2 bone scaffolds. The compressive strength of the scaffold was considered as the maximum stress prior to the failure of the scaffold and was defined as the maximum stress detected within the linear elasticity phase before reaching the plateau phase and the subsequent densification of collapsed struts.

2. Material & methods

2.1. Scaffold production

Polymer replication method was used to fabricate doped TiO_2 bone scaffolds as previously described [5,21]. In short, a slurry that contained 65 g anatase TiO_2 powder (HOMBITAN FF-Pharma, Sachtleben Chemie GmbH, Duisburg, Germany) and 25 mL 0.1 M $CaCl_2$ or $SrCl_2$ salt solution, was stirred at 5000 rpm for 2.5 h at 15−17 °C (Dispermat Ca-40, VMA-Gertzmann GmbH, Reichshof, Germany) with a HCl-adjusted work pH of 1.5−1.7. Polymer foams (60 ppi, diameter 10 mm, height 10 mm; Bulbern S, Eurofoam GmbH, Wiesbaden, Germany) were coated with the slurry and dried for 24 h at room temperature. After burn out of the polymer at 450 °C, the scaffolds were sintered at high temperature. To investigate the influence of sintering parameters on doped TiO_2 grain boundaries, heating rate (1.5-12 K/min), holding time (3-40 h), holding temperature (1450−1600 °C) and cooling rate (air quechning-5 K/min) were changed one parameter at the time.

To investigate the influence of the sintering environment on $SrTiO_3$ formation, different ovens with different features were used. Oven A (HTC08/16, Nabertherm, Germany) exhibited open silicon carbide heating rods and aluminium silicate insulation and did not have an active cooling system. The maximum heating temperature was 1500 °C. Oven B (LHT02/17 LB, Nabertherm, Germany) had insulated heating rods, and therefore, only aluminium silicate within the furnace chamber, but exhibited an active cooling system. Additionally, the maximum heating temperature was higher compared to oven A at 1600 °C.

2.2. Corrosion test

A corrosion test was performed using the differently sintered scaffolds. Scaffolds were stored for 24 h in 1 mM HCl solution in polypropylene tubes at 37 °C. Additionally the strongest Sr-doped scaffolds were exposed to an acidic 1 mM HCl solution for 4 weeks at 37 °C. Before further investigation of the scaffolds, dH_2O rinsing and drying for 24 h at 37 °C was carried out.

2.3. Mechanical properties

To compare mechanical properties of the corroded and uncorroded scaffolds, their compressive strength was measured. Measuring the compressive strength of highly porous brittle ceramics is challenging due to uneven stress distribution caused by the irregular strut architecture and uneven contact with the testing device [22]. Therefore, the scaffolds were placed between two 2 mm silicone rubber discs acting as compliant padding to ensure a more uniform load distribution. Using a uniaxial mechanical testing machine (Zwick/Roell Z2.5; Zwick GmbH & Co. KG, Ulm, Germany) equipped with a 1 kN load cell, scaffolds were compressed along their long axis with a preload of 0.5 N and testing speed of 100 mm/min. The test was performed until failure of the scaffold, manifested by a plateau region in the compressive stress-strain curve. Compressive strength of the scaffold was defined as the peak stress within the linear elastic region in the compressive stress-strain curve measured for each sample. A representative stress-strain curve is shown in Fig. 1. Test Expert II software (Zwick, Germany) was used to calculate the compressive strength based on the scaffold diameter.

2.4. Scaffold properties

Microcomputed tomography (SkyScan1172, Bruker microCT, Kontich, Belgium) was used to determine the 3D scaffold parameters strut thickness, pore size, porosity and interconnectivity of open pores. Five scaffolds (n = 5) were placed in a plastic holder and by using a voltage of 100 kV, current of 100 µA, 6 µm voxel and 0.5 mm aluminium filter, three x-ray absorption images were taken every 0.4° up to a total of 180°. For reconstruction of a 3D model and calculation of parameters, the Skyscan softwares NRecon, CTan and CTvox (Bruker, Billerica, USA) were used.

2.5. Scanning electron microscopy (SEM) and energy dispersive X-ray spectroscopy (EDX)

For the visual characterization of the grain boundaries in uncorroded and corroded scaffolds fabricated with different sintering parameters, a field emission scanning electron microscope (FE-SEM, S-4800, Hitachi, Japan) was used. Scaffolds were cut to 2 mm slices and attached on the sample holder with epoxy resin (Poxy Pak™ Epoxy, Ted Pella, Inc., Sweden) mixed with 50 wt.% carbon powder (PELCO® Carbon (Graphite) Powder, Ted Pella, Inc., Sweden). Scaffolds were carbon-coated (Edwards AUTO 306, Crawly, UK) prior to SEM imaging.

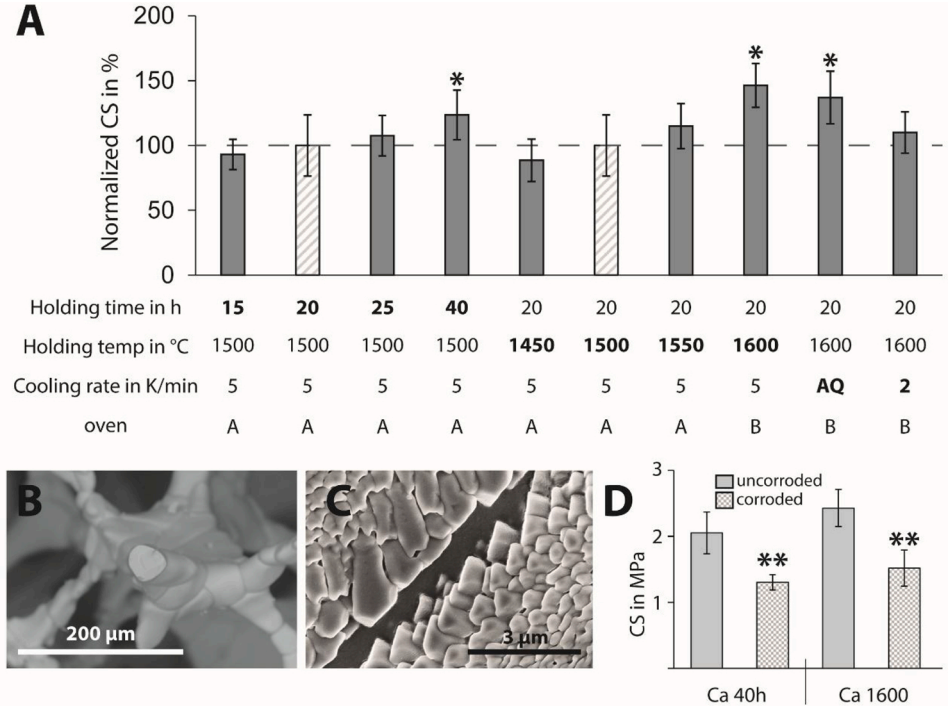

Fig. 2. Overview of important scaffold properties for Ca doped scaffolds. The compressive strength (CS) of the control scaffolds used for normalization is highlighted with a different bar fill. The compressive strength overview shows a significant increase in strength for a long sintering time (40 h), high sintering temperature (1600 °C) and fast cooling rate (air quenching: AQ) (A). Dense struts causing the high compressive strength for the Ca-doped scaffolds sintered for 40 h (B). Corroded grain boundaries and characteristic TiO_2 lamellae in Ca-doped scaffolds sintered at 1600 °C (C). Scaffolds with the highest measured compressive strength showed significant loss of compressive strength after 24 h in 1 mM HCl solution (D). *$p < 0.05$ compared to control scaffolds, **$p < 0.05$ compared to uncorroded scaffolds, $n = 10$.

Secondary electrons generated at an acceleration voltage of 5 kV were used to image the scaffold surface at a working distance of approximately 9 mm. Additionally, the combination of SEM and Quantax EDS system with XFlash® 4030 detector (Bruker AXS Microanalysis, Germany) was used to qualify chemical composition within the grain boundaries.

2.6. Statistical analysis

Statistical analysis for microCT data (strut thickness, pore size, porosity and interconnectivity) was performed using one-way analysis of variance (ANOVA) and pairwise multiple comparison by using Holm-Sidak method. The overall significance level was $p < 0.05$ and $n = 5$. The results of the compressive strength test are normalized to the control scaffolds sintered using previously established standard sintering conditions [12] and shown as mean ± standard deviation. Statistical analysis was performed using one-way ANOVA with ad hoc pairwise multiple comparison by using the Holm-Sidak method. Statistical significance was considered at $p < 0.05$ and $n = 10$ for compressive strength analysis.

3. Results & discussion

3.1. Ca-doped TiO_2 scaffolds

When using the polymer replica method, the compressive strength of the fabricated highly porous TiO_2 scaffolds has been shown to be influenced mainly by changes in their strut morphology [5,21]. As shown in a previous study, the densification of the strut morphology observed in both Ca- and Sr-doped TiO_2 scaffolds result in a significant increase in compressive strength of these scaffolds in comparison to the undoped control scaffolds [21]. Furthermore, different sintering mechanisms present in the differently doped TiO_2 ceramics were observed to influence the densification of the material during sintering, and thus, directly influence the strut morphology [21]. Densification of the ceramic takes place during the second stage of sintering, where necks between particles are forming and crystal growth is dominant [23–26]. Further densification can also occur by elimination of closed micro-pores present in the grain boundaries [26]. As shown in Fig. 2A, Ca-doped TiO_2 scaffolds showed a gradually increased compressive strength as the sintering time was prolonged from 15 h up to 40 h, resulting in statistically significant increase in strength for scaffolds sintered for the longest time of 40 h. Regarding TiO_2 scaffolds, a correlation between sintering time and compressive strength was described by Tiainen et al. [5]. For undoped TiO_2 scaffolds, a maximum compressive strength was reached after 20 h sintering and no further increase in strength was observed for longer sintering times. Thus, an optimal sintering time of 20 h was determined and further densification did not result in further increase of compressive strength for undoped TiO_2 scaffolds. In contrast, Ca-doped TiO_2 showed different densification mechanisms compared to the undoped TiO_2 scaffolds. Ca-doped scaffolds showed denser struts because of the elimination of hollow spaces within the struts, which is a result of the production method. These denser struts, as shown in Fig. 2B, are leading to significantly higher strut strength, which was described before [21]. Prolonging the sintering time from 20 h to 40 h for Ca-doped TiO_2 resulted in further densification of the ceramic during sintering, resulting in further significant increase in compressive strength of the produced scaffolds.

Similar to the sintering time, higher sintering temperatures were also shown to result in progressively higher compressive strength with the highest sintering temperature (1600 °C) yielding scaffolds with significantly increased compressive strength compared to the control scaffolds sintered at 1500 °C (Fig. 2A). During sintering at higher temperatures, the self-diffusion coefficient is increased and leads to higher densification [23]. Moreover, the added dopants and impurity atoms from the sintering environment segregate to the grain boundaries, which at high temperatures form a liquid phase that contributes to the increased densification of the material at higher sintering temperatures. As the sintering temperature was increased from 1500 °C to 1600 °C, more liquid phase is likely to form at the grain boundaries [27], resulting in enhanced viscous flow, and thereby, densification during sintering. As previously shown, impurities, such as silicates originating from the sintering environment, can further contribute to the formation of a liquid phase at the grain boundary region and thus enhance the densification of polycrystalline ceramics [11,28,29]. While no statistically significant difference was observed in porosity and interconnectivity of

Table 1
Scaffold parameters strut thickness, pore size, porosity and interconnectivity of different sintered Ca-doped TiO_2 scaffolds. Parameters were calculated on the basis of a 3D microCT model.

	Strut thickness µm	Pore size µm	Porosity %	Interconnectivity for a connection size of minimum 118 µm %
Ca-1500−5	55 ± 3	457 ± 5	92 ± 1	99 ± 0
Ca-1500−40h	58 ± 6	438 ± 9	92 ± 1	99 ± 0
Ca-1600-AQ	60 ± 5	414 ± 13	91 ± 1	99 ± 0

* $p < 0.05$, $n = 5$.

differently sintered scaffolds, smaller pore sizes were observed for scaffolds sintered at higher temperatures (Table 1). Together with the observed 8% reduction in overall scaffold dimensions, the combination of smaller pore sizes and thicker struts while porosity and interconnectivity remained unchanged indicates increased material densification when sintering temperature was increased. Thus, the more dominant liquid phase led to higher densification and resulted in higher compressive strength in scaffolds sintered at 1600 °C.

However, the occurrence of a liquid phase during sintering can cause the formation of a glassy phase in the intergranular regions that dominates the mechanical properties of the grain boundaries, and thereby, the strength of the fabricated scaffolds. When exposed to acidic environments, undoped TiO_2 scaffolds were shown to corrode at the grain boundaries and the dissolution of their amorphous grain boundary consisting mostly of phase was shown to result in a dramatic loss of compressive strength [11]. An even greater reduction in compressive strength as a result of grain boundary corrosion has previously been observed for TiO_2 scaffolds doped with Ca and Sr [12]. Although the compressive strength of Ca-doped scaffolds could be improved by longer sintering times and higher sintering temperatures in the present study, grain boundary corrosion still caused a significant loss of compressive strength following exposure to 1 mM HCl (Fig. 2C and D). Furthermore, the dissolution of the grain boundary phase in Ca-doped scaffolds was homogenous, and thus, similar compared to the dissolution observed in the undoped control scaffolds. Upon cooling, some of the liquid phase that forms during sintering of Ca-doped TiO_2 scaffolds crystallises as the TiO_2 lamella detected previously and shown in Fig. 2C, while the residual liquid phase forms a Ca- and Si-rich amorphous grain boundary phase between the grains [12]. Because of the homogenous grain boundary dissolution and no change in corrosion resistance between differently sintered Ca-doped scaffolds, the grain boundary phase in Ca-doped scaffolds are assumed to be predominantly amorphous for all tested sintering conditions, as was previously shown for the Ca-doped control scaffolds sintered at 1500 °C for 20 h [12]. The amorphous phase within the grain boundaries is more likely to dissolve in acidic environments, while the presence of a crystalline phase within the grain boundaries would cause inhomogeneous grain boundary dissolution.

When exposed to an acidic environment, hydrogen activity is the driving force for corrosion as non-bridging oxygen atoms in the glassy grain boundary phase are attacked by the H^+ ions [16]. The correlation of increased glass stability by increasing bridging-oxygen atoms was described by Rodrigues et al., who investigated glass stability of devitrite glass ($Na_2Ca_3Si_6O_{16}$) by comparing pure glass and glass mixed with TiO_2 [30]. They showed that the reduction of Na^+ and Ca^{2+} by the replacement with TiO_2 decreased the number of bridging-oxygen atoms and increased the glass stability. Considering the grain boundary phase composition in this study, segregation of calcium ions at the grain boundaries is likely to decrease the number of bridging oxygen atoms in the amorphous Si-rich grain boundary phase and reduce the stability of the glassy phase in an acidic environment. Consequently, the decreased glass stability in the amorphous Ca-rich grain boundary phase caused higher corrosion and a significant decrease in compressive strength,

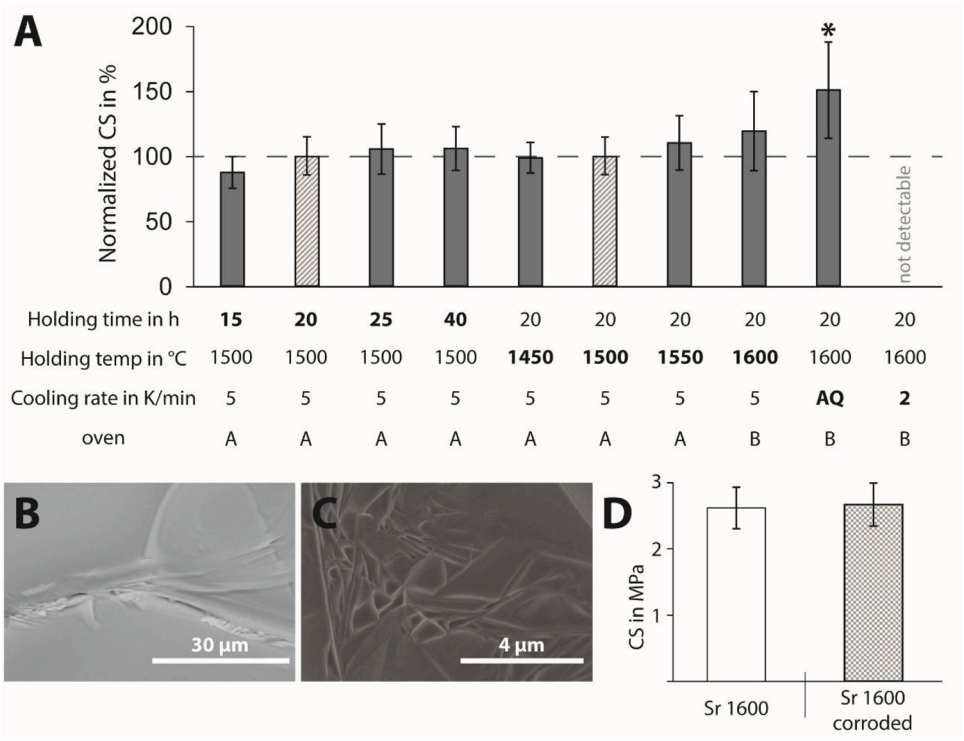

Fig. 3. Overview of important scaffold properties of Sr doped scaffolds. The compressive strength (CS) of the control scaffolds used for normalization is highlighted with a different bar fill. Scaffolds with the fastest cooling rate (AQ) showed significantly higher compressive strength (A). Scaffolds with a slow cooling rate showed crystal formation and the presence of hollow spaces within grain boundaries (B). AQ scaffolds showed corroded grain boundaries (C), but the crystal formation led to stable compressive strength of scaffolds after corrosion (D). *$p < 0.001$ compared to control scaffolds, $n = 10$.

Table 2
Scaffold parameters strut thickness, pore size, porosity and interconnectivity of different sintered Sr-doped TiO_2 scaffolds. Parameters were calculated on the basis of a 3D microCT model.

	Strut thickness µm	Pore size µm	Porosity %	Interconnectivity for a connection size of minimum 118µm %
Sr-1500−5	58 ± 2	411 ± 29	92 ± 1	99 ± 0
Sr-1600-AQ	62 ± 7	378 ± 6*	91 ± 1	99 ± 0

* $p < 0.05$, $n = 5$.

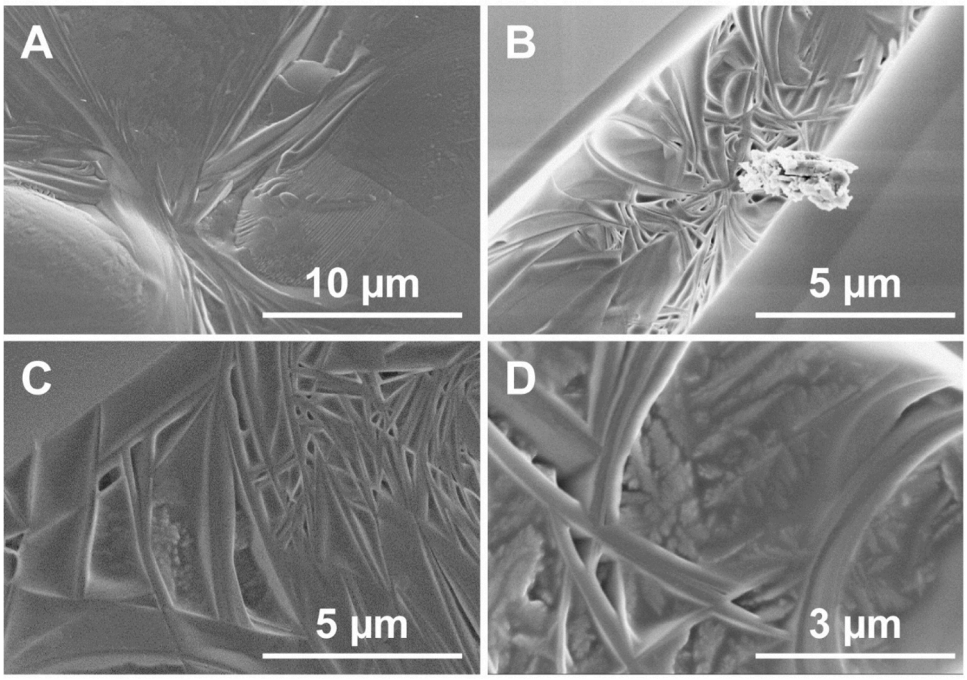

Fig. 4. $SrTiO_3$ crystals in corroded Sr-doped TiO_2 scaffolds sintered and cooled down with 1500 °C and 5 K/min (A), 1600 °C and 5 K/min (B), 1600 °C and AQ (C). More and smaller $SrTiO_3$ crystals in 1600-AQ scaffolds are shown more in detail (D).

irrespective of the applied sintering conditions.

3.2. Sr-doped TiO_2 scaffolds

Sr-doped scaffolds showed significant increase in compressive strength for the highest sintering temperature of 1600 °C and very fast cooling rate (air quenching) while the porosity and interconnectivity remained unchanged, as shown in Fig. 3A and Table 2.

The higher sintering temperature resulted in more liquid phase present at the grain boundary regions during sintering, while the rapid cooling hindered the growth of the $SrTiO_3$ crystals forming during cooling of the material. This resulted in the formation of an interconnected crystalline $SrTiO_3$ network embedded in an amorphous Si- and Sr-rich phase at the grain boundaries of the Sr-doped scaffolds the scaffold sintered. For Ca-doped scaffolds, elimination of micropores in the amorphous grain boundary phase was shown to be the most

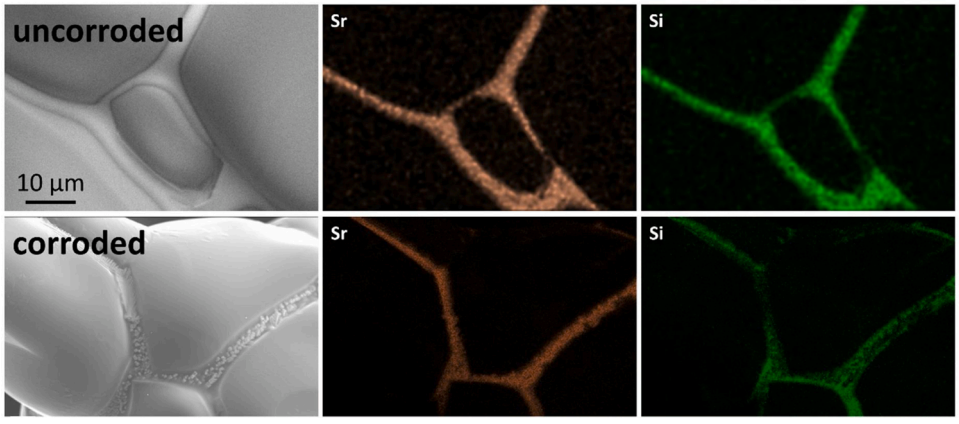

Fig. 5. SEM and EDX images of corroded and uncorroded grain boundaries in Sr-doped scaffolds show the remaining phase within doped grain boundaries after corrosion.

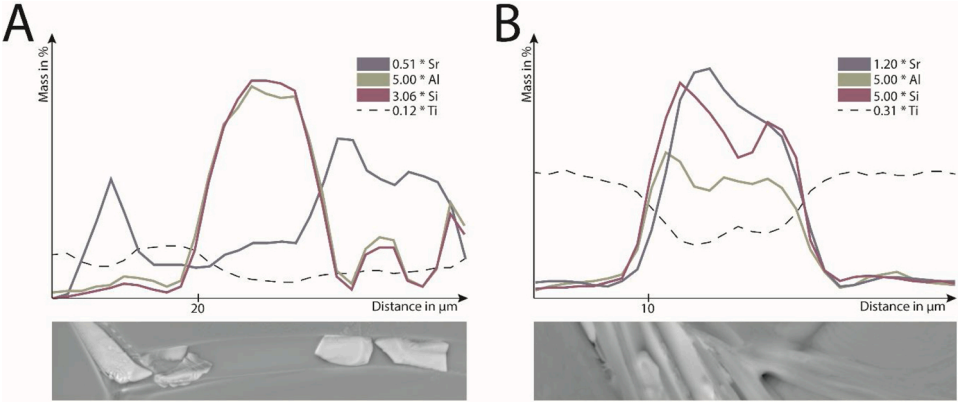

Fig. 6. Corroded grain boundaries in Sr-doped TiO_2 scaffolds. While Sr peaks represented $SrTiO_3$ crystals, Al and Si peaks showed the amorphous phase within the grain boundaries (A). Differences in crystal formation caused by sintering conditions could not be observed (B).

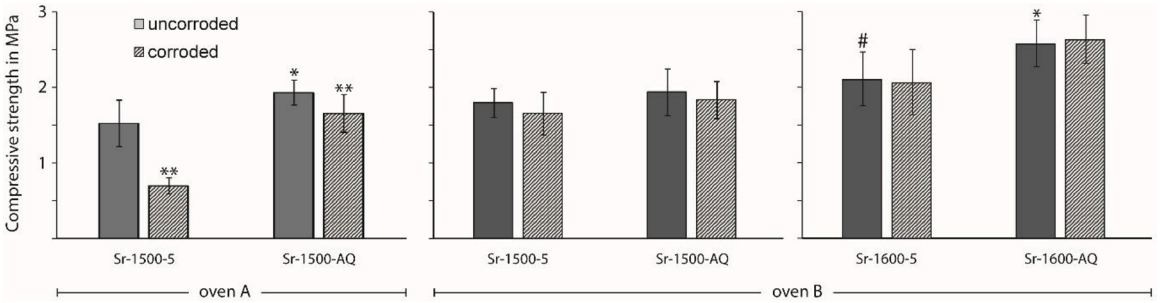

Fig. 7. Compressive strength of corroded and uncorroded Sr-doped TiO_2 scaffolds sintered in different ovens. Statistical significance ($p < 0.001$, $n = 10$) is indicated in comparison to 5 K/min using the same oven and same temperature (*), uncorroded scaffolds (**) and the comparison between B-1500-5 and B-1600-5 (#). 1500 and 1600 indicates the sintering temperature and 5 or AQ indicates the cooling rate.

important factor influencing their compressive strengths. In contrast, Sr-doped scaffolds showed two important changes in the microstructure of the material which influenced the compressive strength. First, the material densification was observed to be higher at higher sintering temperatures, resulting in a significantly smaller pore size. Second, the formation of a $SrTiO_3$ crystal network at the grain boundaries seemed to influence the compressive strength significantly in Sr-doped scaffolds. Slow cooling rates led to the formation of large intergranular $SrTiO_3$ crystals (Fig. 3B), which resulted in very low compressive strength (< 0.5 MPa) already before any corrosion had occurred. In contrast, air quenching caused the formation of very small crystals and a significant increase in compressive strength which maintained after corrosion (Fig. 3C and D). As shown in Fig. 3, the increase in sintering temperature from 1500 °C to 1600 °C appeared to result in a more optimal nucleation condition for $SrTiO_3$ as several more crystals were present in the samples sintered at higher temperature (Fig. 4B). The crystal growth was mainly influenced by the cooling rate. Consequently, Sr-doped scaffolds sintered at 1500 °C and cooled with a cooling rate of 5 K/min showed less and larger crystals (Fig. 4A) than the scaffolds sintered at 1600 °C and that were air quenched, for which a large number of smaller crystals were present (Fig. 4C and D).

While the crystal formation had a strong influence on the compressive strength of the scaffolds, the sintering environment, and especially, the amount of impurities present during sintering affected the corrosion behaviour. A corrosion resistant crystalline phase was observed within the grain boundaries of scaffolds exposed to 1 mM HCl, while the acidic environment resulted in dissolution of amorphous silicon and aluminium-rich grain boundary phase. This remaining phase within corroded Sr-doped grain boundaries is shown in Fig. 5.

The strong Sr signal observed in the EDX spectra suggests that this corrosion resistant phase consists of $SrTiO_3$ (Fig. 6A). This is in accordance with our previous findings that identified the formation of crystalline $SrTiO_3$ at the grain boundaries of Sr-doped TiO_2 scaffolds [12]. Thus, SEM images show the resistant crystalline $SrTiO_3$ phase that remains in the grain boundaries after the Si and Al-rich amorphous phase has dissolved (Fig. 6). However, the detection of differences in crystal formation caused by a change in sintering conditions was not possible due to the limited spatial resolution of the EDX spectrum (Fig. 6B).

As shown in Fig. 7, corrosion was present in Sr-doped scaffolds sintered in oven A, which has open heating rods, and thus, higher impurity contents. Sr- doped scaffolds sintered in oven B, which has insulated heating rods, did not show a decrease in compressive strength caused by corrosion. This leads to the assumption that a higher amount of Si that originates from the sintering environment was present during sintering and resulted in a more dominant Si-rich amorphous phase within the grain boundaries of the fabricated TiO_2 scaffolds. The dissolution of this dominant Si-rich phase resulted in a significant loss of compressive strength after exposure to an acidic environment. Furthermore, the dominant Si-rich phase influenced the crystal formation of $SrTiO_3$ within the grain boundaries and a lower compressive strength compared to scaffolds sintered in oven B with unexposed Si-rich heating rods was observed. However, the formation of $SrTiO_3$ within the grain boundaries of scaffolds sintered in an environment rich in Si did not result in the formation of a crystalline network which could maintain the high compressive strength of the scaffold after corrosion. Thus, the dissolution of the amorphous phase between the $SrTiO_3$ crystals showed to dominate the corrosion behaviour in Sr-doped scaffolds sintered in oven A. In contrast, the formation of $SrTiO_3$ in a sintering environment with reduced impurity content is likely to cause formation of less Si-rich phase and a more dominant crystalline $SrTiO_3$ phase within the grain boundaries. Consequently, the network of $SrTiO_3$ crystals within the

grain boundaries was shown to be more corrosion resistant. Although the amorphous phase within the grain boundary phase is readily dissolved after exposure to an acidic environment, the crystalline $SrTiO_3$ network resulted in a stable compressive strength in the fabricated Sr-doped scaffolds. This assumption is further supported by another study that has shown a suppressed $SrTiO_3$ crystal growth caused by the present dopants [31].

4. Conclusion

The high amount of Ca in Ca-doped TiO_2 scaffolds was shown to influence the glassy phase present in the grain boundaries. Ca as a glass modifier appeared to prevent crystallization of the grain boundary phase. The resulting amorphous grain boundary phase dissolved after exposure to an acidic environment and resulted in a significant loss in compressive strength of Ca-doped scaffolds. In contrast, Sr-doped TiO_2 scaffolds exhibited $SrTiO_3$ crystals within their grain boundaries. Due to higher sintering temperature, faster cooling rate and a reduction of impurities in the sintering environment, a network of $SrTiO_3$ crystals within grain boundaries was formed and led to increased compressive strength that was maintained even after corrosion.

The improved Sr-doped scaffolds, fabricated with optimised sintering conditions, maintained their high compressive strength up to 4 weeks after exposure to a corrosive media. Especially for the use as bone grafts, Sr-doped scaffolds can guarantee the necessary mechanical support during bone regeneration, despite the acidic physiological environment that may be present during inflammation. Furthermore, corrosion resistant ceramic foams may also be of special interest for other applications such as filters or catalysts in corrosive environments.

Declaration of Competing Interest

The authors declare that they have no known competing financial interests or personal relationships that could have appeared to influence the work reported in this paper.

References

[1] L. Zhang, T. Kanki, N. Sano, A. Toyoda, Development of TiO2 photocatalyst reaction for water purification, Sep. Purif. Technol. 31 (1) (2003) 105–110.
[2] E. Watanabe, M. Fukaya, H. Taoda, Generation of low-molecular-weight organic compounds in water by titania photocatalyst under UV-Vis light radiation, Res. Chem. Intermed. 34 (4) (2008) 365–374.
[3] J.M. Dostanić, D.R. Lončarević, P.T. Banković, O.G. Cvetković, D.M. Jovanović, D.Ž. Mijin, Influence of process parameters on the photodegradation of synthesized azo pyridone dye in TiO2 water suspension under simulated sunlight, J. Environ. Sci. Health, Part A 46 (1) (2011) 70–79.
[4] T. Nonami, H. Hase, K. Funakoshi, Apatite-coated titanium dioxide photocatalyst for air purification, Catal. Today 96 (3) (2004) 113–118.
[5] H. Tiainen, D. Wiedmer, H.J. Haugen, Processing of highly porous TiO_2 bone scaffolds with improved compressive strength, J. Eur. Ceram. Soc. 33 (1) (2013) 15–24.
[6] A. Verket, B. Müller, J.C. Wohlfahrt, S.P. Lyngstadaas, J.E. Ellingsen, H.J. Haugen, H. Tiainen, TiO_2 scaffolds in peri-implant dehiscence defects: an experimental pilot study, Clin. Oral Implants Res. 27 (10) (2016) 1200–1206.
[7] R. Sabetrasekh, H. Tiainen, S.P. Lyngstadaas, J. Reseland, H. Haugen, A novel ultra-porous titanium dioxide ceramic with excellent biocompatibility, J. Biomater. Appl. 25 (6) (2011) 559–580.
[8] M. Gómez-Florit, M. Rubert, J.M. Ramis, H.J. Haugen, H. Tiainen, S. P. Lyngstadaas, M. Monjo, TiO2 scaffolds sustain differentiation of MC3T3-E1 cells, J. Biomater. Tissue Eng. 2 (4) (2012) 336–344.
[9] J. Forsgren, F. Svahn, T. Jarmar, H. Engqvist, Formation and adhesion of biomimetic hydroxyapatite deposited on titanium substrates, Acta Biomater. 3 (6) (2007) 980–984.
[10] H. Tiainen, J.C. Wohlfahrt, A. Verket, S.P. Lyngstadaas, H.J. Haugen, Bone formation in TiO_2 bone scaffolds in extraction sockets of minipigs, Acta Biomater. 8 (6) (2012) 2384–2391.
[11] B. Müller, H. Haugen, S.L. Simonsen, H. Tiainen, Grain boundary corrosion of highly porous ceramic TiO_2 foams is reduced by annealing and quenching, J. Eur. Ceram. Soc. 36 (1) (2016) 179–188.
[12] A. Klemm, M. Gomez-Florit, P.A. Carvalho, M. Wachendörfer, M.E. Gomes, H. J. Haugen, H. Tiainen, Grain boundary corrosion in TiO2 bone scaffolds doped with group II cations, J. Eur. Ceram. Soc. 39 (4) (2019) 1577–1585.
[13] S.H. Ralston, Bone structure and metabolism, Medicine 41 (10) (2013) 581–585.
[14] I. Silver, R. Murrills, D. Etherington, Microelectrode studies on the acid microenvironment beneath adherent macrophages and osteoclasts, Exp. Cell Res. 175 (2) (1988) 266–276.
[15] K.R. Mikeska, S.J. Bennison, S.L. Grise, Corrosion of ceramics in aqueous hydrofluoric acid, J. Am. Ceram. Soc. 83 (5) (2000) 1160–1164.
[16] W.B. White, Theory of corrosion of glass and ceramics, Corrosion of glass, ceramics and ceramic superconductors (1992) 2–28.
[17] B. Müller, H. Haugen, O. Nilsen, H. Tiainen, Atomic layer deposited TiO2 protects porous ceramic foams from grain boundary corrosion, Corros. Sci. 106 (2016) 35–42.
[18] B. Seipel, K.G. Nickel, Protection of silicon nitride ceramics against corrosion in acidic aqueous solutions by enforced internal passivation, Ceram. Int. 30 (2) (2004) 267–271.
[19] K. Gavrilov, S.J. Bennison, K.R. Mikeska, J.M. Chabala, R. Levi-Setti, Silica and magnesia dopant distributions in alumina by high-resolution scanning secondary ion mass spectrometry, J. Am. Ceram. Soc. 82 (4) (1999) 1001–1008.
[20] H. Klemm, Silicon nitride for high-temperature applications, J. Am. Ceram. Soc. 93 (6) (2010) 1501–1522.
[21] A. Klemm, H. Tiainen, Coagulated concentrated anatase slurry leads to improved strength of ceramic TiO_2 bone scaffolds, Ceram. Int. 44 (6) (2018) 6265–6271.
[22] M. Mehr, C. Davis, K. Sadman, R.J. Hooper, M.V. Manuel, J.C. Nino, Epoxy interface method enables enhanced compressive testing of highly porous and brittle materials, Ceram. Int. 42 (1B) (2016) 1150–1159.
[23] C.B. Carter, M.G. Norton, Ceramic Materials: Science and Engineering, Springer, 2007.
[24] M.N. Rahaman, Ceramic Processing and Sintering, CRC press, 2017.
[25] O.-H. Kwon, Liquid Phase Sintering: Ceramics, Encyclopedia of Materials: Science and Technology, 2001.
[26] H. Tanaka, A. Yamamoto, J.-i. Shimoyama, H. Ogino, K. Kishio, Strongly connected ex situ MgB_2 polycrystalline bulks fabricated by solid-state self-sintering, Supercond. Sci. Technol. 25 (11) (2012), 115022.
[27] V. Daněk, I. Nerád, Phase diagram and structure of melts of the system CaO—TiO2—SiO2, Chem. Pap. 56 (4) (2002) 241–246.
[28] J.-H. Park, Densification and mechanical properties of titanium diboride with silicon nitride as a sintering aid, J. Am. Ceram. Soc. 82 (11) (1999) 3037–3042.
[29] G. Brahma Raju, B. Basu, Densification, sintering reactions, and properties of titanium diboride with titanium disilicide as a sintering aid, J. Am. Ceram. Soc. 90 (11) (2007) 3415–3423.
[30] A. Rodrigues, L. Silva, R. Zhang, V. Soares, Structural effects on glass stability and crystallization, CrystEngComm 20 (16) (2018) 2278–2283.
[31] S.-Y. Chung, D.Y. Yoon, S.-J.L. Kang, Effects of donor concentration and oxygen partial pressure on interface morphology and grain growth behavior in SrTiO3, Acta Mater. 50 (13) (2002) 3361–3371.